Effects of Ligand−Receptor Geometry and Stoichiometry on Protein-Induced Aggregation of Biotin-Modified Colloidal Gold

Stephen Connolly, Stephen Cobbe, and Donald Fitzmaurice*

Department of Chemistry, University College Dublin, Belfield, Dublin 4, Ireland

Received: May 26, 2000; In Final Form: December 6, 2000

Colloidal gold nanoparticles have been modified with a biotin analogue (DSDA). On addition of streptavidin, a biotin-binding protein, nanoparticle aggregation is observed. The extent and rate of aggregation depend on the relative concentrations of gold nanoparticles, DSDA, and streptavidin. To explain these effects, a model has been developed. This model is an extension of both the classical Smoluchowski model of aggregation and the recently developed model of linker induced aggregation (Kisak et al.). The inclusion of geometric and steric factors in our model explains several features that are relevant with our gold particles. The essential differences between our system and that of Kisak et al. are discussed as well as possible future areas of study.

Introduction

Colloidal aggregation, induced by specific biological interactions, is attracting increased attention as a self-assembly process for building of complex nanostructures.[1−7] As already mentioned by Kisak et al, one of the main reasons for this interest is the possibility for controlled aggregation which are opened up by the specificity of the biological interactions.[6]

To maximize the usefulness of specific interactions in controlling aggregation; it is necessary to have a model for this class of aggregation. The system under study[8,9] consists of gold nanocrystals modified by a biotin analogue, which are specifically aggregated in the presence of streptavidin.[10,11] This system provides particular opportunities for both the development and testing of aggregation models.

The results obtained highlight the essential difference between the gold nanoparticle system under study and a related vesicle system developed by Kisak et al.[6,8,9] In our view, the key difference between these two systems is that, in the case of the gold nanocrystals, there is very little scope for lateral diffusion of the surface bound streptavidin. In the Kisak system, where the streptavidin is bound to a lipid bilayer, one would expect significant lateral diffusion. Because of this difference, one would expect the gold aggregates to be diffuse, while one would expect the vesicle aggregates to be compact (as they can rearrange through the lateral surface diffusion already mentioned). This is indeed what is observed.

Other differences concern the size of the nanoparticles (∼16 nm diameter gold nanocrystals versus ∼100 nm diameter vesicles) and the maximum surface coverage of streptavidin (∼50 streptavidins/gold nanocrystal compared with ∼10−15 streptavidins/vesicle).[6,8,9] In our system we see a second-order effect in the probability of sticking for a collision between two nanoparticles; such an effect would be most apparent when dealing with large particles at high surface coverages of streptavidin and as such would not be expected for the Kisak system.

* To whom correspondence should be addressed.

SCHEME 1: Synthesis of DSDA

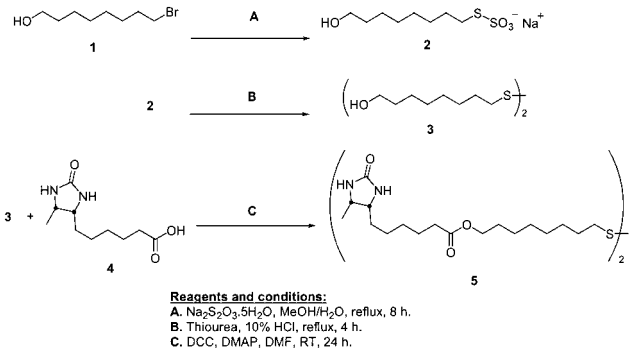

Experimental Section

All chemicals were used as supplied by the Sigma-Aldrich Chemical Co. Ltd. Distilled deionized Millipore-MilliQ water was filtered through a 0.02 μm inorganic Anotop filter and was used to prepare all solutions.

Preparation of the Disulfide Desthiobiotin Analogue. The disulfide desthiobiotin analogue was synthesized according to Scheme 1. 8-Bromooctan-1-ol (**1**) and desthiobiotin (**4**) were used as supplied.

Sodium Thiosulfonate *S*-(8-Hydroxyoctyl) Ester (2). 1 (24.2 mmol, 5.051 g) was dissolved in methanol (29 mL) to which water was added dropwise until the development of a slight turbidity.[12] This solution was heated to reflux, at which point sodium thiosulfate pentahydrate (29.9 mmol, 7.430 g) in water (6 mL) was added dropwise over a period of 1 h. After a further 8 h of reflux, the reaction mixture was allowed to cool to room temperature before reducing to dryness on a rotary evaporator, yielding 6.61 g of the crude Bunte salt. The product was used as is in the subsequent reaction, and as such no elemental analyses were obtained.

8-(8-Hydroxyoctyldisulfanyl)octan-1-ol (3). 2 (13.7 mmol, 3.64 g) and thiourea (13.7 mmol, 1.05 g) were added to a 10% solution of hydrochloric acid in water (70 mL) and refluxed for 4 h, filtered, and recrystallized (×2) from a mixture of

10.1021/jp001948i CCC: $20.00
Published on Web 02/24/2001

hexane and chloroform (according to the following procedure: the crude compound was suspended in hexane at its boiling point, chloroform was added, at its boiling point, dropwise until the entire compound had dissolved, and the solution was then filtered hot and allowed to cool slowly, resulting in the crystallization of the compound), to yield 2.15 g of the product (**3**) as a white powder (yield 97%).

Anal. Calcd for $C_{16}H_{34}O_2S_2$: C, 59.6; H, 10.6; S, 19.9; O, 9.9. Found: C, 59.4; H, 10.6; S, 20.3; O, 9.6.

^{1}H 270 MHz NMR ($CDCl_3$; ppm): 1.2−1.5 (m, 24H, CH_2); 2.72 (t, 4H, J = 7.42 Hz, CH_2SS); 3.68 (t, 4H, J = 6.60 Hz, CH_2OH).

6-(5-Methyl-2-oxoimidazolidin-4-yl)hexanoic Acid 8-{8-[6-(5-Methyl-2-oxoimidazolidin-4-yl)hexanoyloxy]octyldisulfanyl}-octyl Ester (DSDA) (5). 1,3-Dicyclohexylcarbodiimide (2.23 mmol, 0.461 g) was dissolved in dry DMF (5 mL). To this clear solution was added **4** (2.05 mmol, 0.438 g) followed by 4-(*N*,*N*-dimethylamino)pyridine (0.09 mmol, 0.010 g) and finally **3** (0.93 mmol, 0.300 g). The reaction mixture was stirred at room temperature for 24 h, stored at 0 °C for 24 h, filtered, and DMF was removed by vacuum distillation. The crude product was purified by silica column chromatography to yield 0.108 g of the product (**5**) (yield: 16.2%).

Anal. Calcd for $C_{36}H_{66}N_4O_6S_2$: C, 60.5; H, 9.3; N, 7.8; S, 9.0; O, 13.4. Found: C, 58.8; H, 8.9; N, 7.8; S, 8.7; O, 15.6.

^{1}H 500 MHz NMR ($CDCl_3$; ppm): 1.05 (d, 6H, J = 6.2 Hz, CH_3), 1.2−1.6 (m, 36H, CH_2); 2.24 (t, 4H, J = 7.45 Hz, CH_2-$COOCH_2$), 2.61 (t, 4H, J = 7.28 Hz, CH_2SS); 3.63 and 3.76 (m, 4H, $(CH)_2(NH)_2CO$), 3.99 (t, 4H, J = 6.58 Hz, CH_2OCO).

Preparation of Gold Sols. Gold nanocrystal dispersions with narrow size distributions were prepared as previously described.[9]

Modification of Gold Sols. Modification of the gold nanocrystals with DSDA was achieved by addition of a 5 mL aliquot of a 1.55 × 10^{-6} mol dm^{-3} aqueous solution of DSDA to 50 mL of the gold sol and stirring for 30 min.

Preparation of Streptavidin Solutions. Streptavidin (essentially salt free) was dissolved in deionized Milli-Q Millipore water at a concentration of 10 mg mL^{-1}. The activity of the resulting solution was subsequently determined by spectrophotometric titration.[13]

Dynamic Light Scattering. Dynamic light scattering experiments were performed using a Malvern PCS-4700 instrument equipped with a 256-channel correlator. The laser source was the 488.0 nm line of a Coherent Innova-70 Ar ion laser typically at a power of 50 mW. The temperature was maintained at 20 °C ± 0.02 °C by an external circulator. Data treatment was as previously described.[9] Kinetic measurements were performed as follows: All samples were degassed by placing 1.5 mL of sample under vacuum in a 2.5 mL all PP/PE syringe and subjecting to impulses (repeatedly flicking a fingernail and finger at the side of the syringe). Within 1 min of the samples being loaded into the syringes, the two samples were mixed using the apparatus illustrated in Scheme 2, the resulting mixture being injected directly into the light-scattering cell. The total dead-space volume of the mixing apparatus is 0.33 ± 0.03 mL, and the mixing apparatus was flushed with filtered water and dried with filtered air within 1 min of the injection of the sample. Measurements were performed continuously; however, at the initial stages of the aggregation, measurements were recorded every 5 s, and as the aggregation slowed, measurements were recorded every 15, 30, and 60 s. Most aggregations were monitored at a scattering angle of 90° as, within experimental error, no significant angular variation was observed in the range 30−135°.

SCHEME 2: Schematic Representation of the Flow Mixing Apparatus Used for DLS Kinetics Measurements

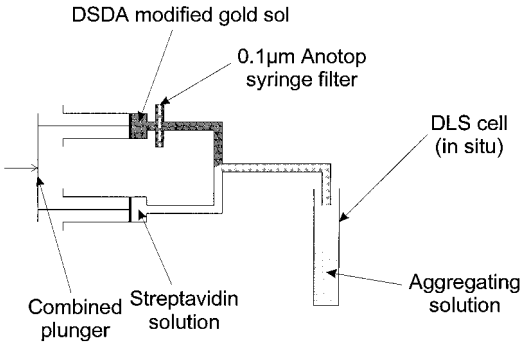

Results and Discussion

The Smoluchowski equation provides the classic description of diffusion-limited aggregation (DLA) in colloids:[14]

$$\frac{dc_k(t)}{dt} = \frac{1}{2}\sum_{1+j=k} K_{ij}c_ic_j - c_k\sum_{1+j=k}^{\infty} K_{kj}c_ic_j \quad k = 1,2, \ldots \infty \qquad (1)$$

Here c_k is the concentration of k-mers and K_{ij}, known as the aggregation kernel, is the rate constant for reaction of i-mers and j-mers to form $(i + j)$-mers. Smoluchowski derived an aggregation kernel on the basis of the Brownian diffusion of aggregates, viz. $K_{ij} \propto (i^{d_f} + j^{d_f})(i^{-d_f} + j^{-d_f})$, where d_f is the fractal dimension, and subsequently made the assumption that this could be approximated by a constant kernel, i.e. where K_{ij} = constant $\forall i,j$, in order to obtain an analytical solution. A constant kernel physically corresponds to the case where all rate constants, for every possible combination of collisions between polymers (aggregates), are the same. The assumption of a constant kernel is reasonably accurate because while $i \approx j$, $K_{ij} \approx$ constant, and the Brownian kernel tends to keep the population profile sufficiently narrow that deviations from the constant kernel approximation are not significant.

With linker-induced aggregation (in both our system and the Kisak system, the linker is streptavidin), the aggregation kernel is modified by a "probability of sticking" factor. When no linkers are bound to particles, the probability of two particles sticking given a collision, P(stick|collide), is zero. As linkers bind to the particles, P(stick|collide) will increase. If a sufficient linker concentration is present then P(stick|collide) will eventually start to decrease toward zero again, corresponding to the case where all the binding sites are occupied by a linker. Accordingly,

$$P(\text{stick}|\text{collide}) = {}^1/_2\alpha(1 - \alpha) \qquad (2)$$

where α is the linker surface coverage. This expression corresponds to that developed by Kisak et al for streptavidin-induced aggregation of biotin-coated vesicles.[6] Briefly, a collision will only stick when it is between a linker-occupied (O) site (probability α) and a linker-unoccupied (U) site (probability $1 - \alpha$). There are four possible arrangements: UU; UO; OU; UU. On summing the favorable probabilities and dividing by the total number of possibilities, one arrives at the above equation.

With aggregation of essentially incompressible gold nanoparticles, however, a second-order effect must be considered; that is, streptavidins adjacent to the point of contact may prevent binding as schematically illustrated in Scheme 3.

Such an effect introduces a $(1 - \alpha^2)$ term for every set of adjacent pairs, n, whose occupancy must be considered. Briefly,

SCHEME 3: Schematic Illustration of How High Surface Coverage of the Linker Group (Streptavidin) Can Physically Prevent Binding Formation by Obstructing Access to the Unbound Sites[a]

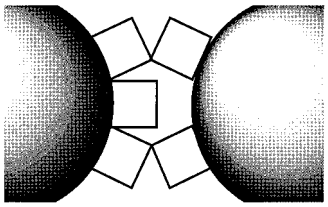

[a] This scheme shows one possible configuration of a collision between two particles where access to the binding site is not possible because of the presence of bound linkers on both particles adjacent to the "point of collision" (although, since the unbound site is inaccessible, there cannot be a "point of collision").

SCHEME 4: Simplified Illustration Showing a Cross Section of the Geometric Analysis of Constraints of Access to Unbound Binding Sites[a]

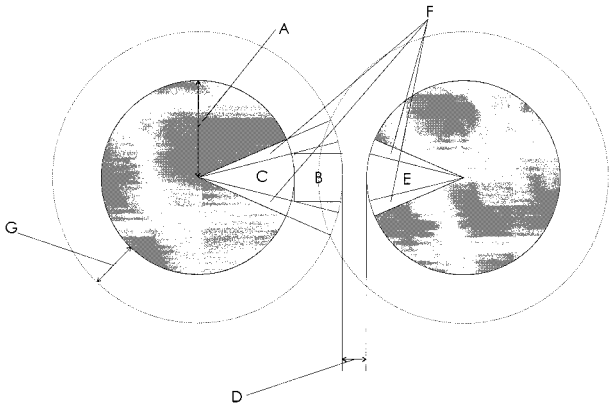

[a] Depending on the dimensions of the particle (gold nanocrystal) and the linker (streptavidin) and the binding site (biotin analogue), varying areas of the surfaces of the two particles cannot be both occupied. Key: (A) particle radius (for our gold nanocrystals: 7.6 nm [9]); (B) linker (for our system: streptavidin, 4.2 × 4.2 × 5.2 nm (see references in ref 9)); (C) solid angle occupied by the linker; (D) the distance at which the linker can bind to the particle (for our system the length of the biotin analogue and the depth of the streptavidin binding site place this value in the range 1.0−2.5 nm); (E) solid angle occupied by the binding site (i.e. this is unoccupied by linker); (F) solid angle whose occupancy affects binding (i.e. the space which cannot be occupied on both particles as it will prevent access to the binding site); (G) length of the linker (for our system we assume the longest length of streptavidin: 5.2 nm). Using an analysis similar to that illustrated, for the gold nanocrystals, streptavidin, and the biotin analogue used in this work, the probability of access to the binding site not being obstructed is given by $(1 - \alpha^2)^n$, where n lies between approximately 0.5 and 1.2. (Note: this calculation must be carried out using solid angles in three dimensions.)

the probability that any two sites are both occupied is given by α^2; therefore, the probability that any two sites are not both occupied is given by $1 - \alpha^2$. Thus, the probability that a configuration as shown in Scheme 3 can occur is given by $^1/_2\alpha(1 - \alpha)(1 - \alpha^2)(1 - \alpha^2)$, where the two $(1 - \alpha^2)$ terms arise because there are two pairs of blocking sites illustrated in Scheme 3. The actual number of blocking sites which must be considered will depend on the geometry of the system under study; e.g., see Scheme 4. Thus we have

$$P(\text{stick}|\text{collide}) = {}^1/_2\alpha(1 - \alpha)(1 - \alpha^2)^n \qquad (3)$$

From the size of the gold particles used in this work and the dimensions of streptavidin and the biotin analogue used, geometric constraints place n between 0.5 and 1.2 (see Scheme 4).

Thus, the Brownian aggregation kernel is given by

$$K_{ij}^{\text{linker}} = \frac{K_{11}^{\text{DLA}}}{4}(i^{d_f} + j^{d_f})(i^{-d_f} + j^{-d_f})P(\text{stick}|\text{collide}) \qquad (4)$$

Such an expression, however, is still restricted by one of the key assumptions of Smoluchowski, viz., that the aggregates are spherical. Such an assumption is perfectly valid for aggregation of vesicles, where the aggregates can rearrange, which is confirmed by their high fractal dimension, 2.9.[6] With the gold particle aggregation considered here, however, such rearrangements are not possible and the aggregates are observed to have a much lower fractal dimension more typical of classical DLA (here, $1.6 < d_f < 2.0$ to within experimental error). With these more tenuous aggregates, a single collision between two aggregates may contain multiple points of contact and will correspondingly increase the overall probability of sticking. We model this effect by using the following form for the aggregation kernel:

$$K_{ij}^{\text{linker}} = \frac{K_{11}^{\text{DLA}}}{4}(i^{d_f} + j^{d_f})(i^{-d_f} + j^{-d_f})(1 - \beta f^{(i,j)}) \qquad (5)$$

Here $\beta = 1 - P(\text{stick}|\text{collide})$ is the probability of not sticking and $f(i,j)$ is the average number of points of contact for an i-mer and a j-mer. Clearly, $f(i,j) \geq 1$, $\partial f(i,j)/\partial i \geq 0$, and $\partial f(i,j)/\partial j \geq 0$. To a first approximation, we represent $f(i,j)$ as a power series in $i + j$, $f(i,j) \approx (1.03)^{i+j}$.

An analytical solution to this aggregation kernel is not possible without significant approximations. Certainly, the Brownian kernel can be replaced by a constant kernel; however, the authors cannot see any method of further simplifying the kernel without losing the properties added. For this reason, the problem was solved numerically using 5th order Runge−Kutta numerical integration.[15] As numerical integration was being used, the Brownian kernel was retained for increased accuracy. The surface coverage, $\alpha(t)$, was modeled as a second-order diffusion-limited reaction between binding sites and streptavidin:

If $[\text{surface sites}]_0 \neq [\text{streptavidin}]_0$

$$\alpha(t) = \frac{[\text{surface sites}]_0 - [\text{surface sites}]_0 e^{k1([\text{streptavidin}]0 - [\text{surface sites}]0)t}}{[\text{surface sites}]_0 - [\text{streptavidin}]_0 e^{k1([\text{streptavidin}]0 - [\text{surface sites}]0)t}} \qquad (6)$$

If $[\text{surface sites}]_0 = [\text{streptavidin}]_0$

$$\alpha(t) = \frac{1}{1 - \dfrac{1}{k_1[\text{surface sites}]_0 t}}$$

$$k_1 = \frac{4000RT(R_{\text{streptavidin}} + R_{\text{particle}})^2}{6\eta \qquad R_{\text{streptavidin}}R_{\text{particle}}} \qquad (7)$$

where $R_{\text{streptavidin}}$ and R_{particle} are the radii of streptavidin and the particles, respectively, R is the gas constant, T is the temperature in Kelvins, and η is the viscosity of the solvent.

A comparison of the actual results of streptavidin-induced aggregation of biotin-derivatized colloidal gold with the theoretically predicted kinetics, for both the modified Smoluchowski

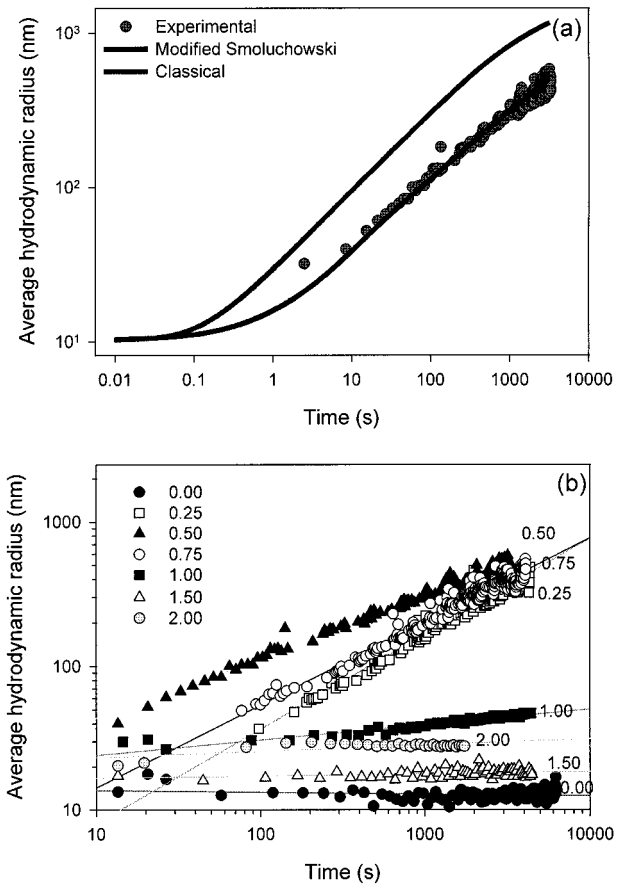

Figure 1. (a) Comparison of actual results of streptavidin-induced aggregation of biotin-derivatized colloidal gold, after addition of 1/2 monolayers of streptavidin, with theoretical predictions from the model developed in this paper and the classical Smoluchowski aggregation model. (b) log−log plot of streptavidin-induced aggregation of DSDA-derivatized gold particles for various concentrations of streptavidin. Streptavidin concentrations are given relative to monolayer coverage. Solid lines represent the linear fit to the log−log plot expected for power-law growth.

(Brownian kernel, eq 5) and classical Smoluchowski (constant kernel) models, is shown in Figure 1. It is worth noting that the only parameter used to fit the data to the curve is the "fractal dimension", as all other parameters are directly related to experimentally obtained values. The fractal dimension only affects the slope of the curve on a log−log plot at late times and is more correctly the hydrodynamic fractal dimension.

The classical Smoluchowski model shows a significant deviation from both the experimental results and the modified model using eq 5; this is associated with the lag time for binding of the linker to the surface of the particles. The classical Smoluchowski model assumes that the particles are "instantly sticky", while, in the case of linker induced aggregation, the particles only "become sticky" when the linker has bound. The time it takes for the particles to become sticky is the lag time.

At early times, the experimental results deviate from those predicted by the modified model (eq 5); while the deviation is only one experimental point at early times, this data point is always there and our explanation for this deviation is incomplete mixing, as follows. Using our flow mixing method, it is clear that the samples are macroscopically mixed. It is unreasonable, however, to expect microscopically perfect mixing. Thus, we expect to see regions of particles adjacent to regions of protein. Initially particles on the boundary of these two regions will bind protein, forming a protein-depleted zone between the particle-rich region and the protein-rich region. On average half of the

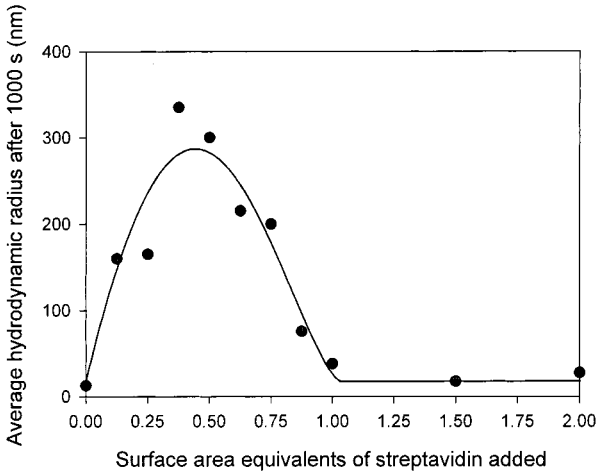

Figure 2. Average hydrodynamic radius, for streptavidin-induced aggregation after 1000 s, as a function of concentration of streptavidin relative to monolayer coverage. The solid line represents the best fit of the data to $x_0 + 2x_1 \min(c_{st}/x_2,1)(1 - \min(c_{st}/x_2,1))(1- \min(c_{st}/x_2,1)^2)^{x3}$, where c_{st} is the concentration of streptavidin − the independent variable, x_0 corresponds to the unaggregated particle size, x_1 is an arbitrary scaling factor, x_2 is the maximum surface coverage, and x_3 is the number of sites neighboring the point of contact which can prevent binding.

TABLE 1: Parameters Resulting from the Least-Squares Fit in Figure 2

param[a]	fit	param[a]	fit
x	20 ± 5 nm	x_2	1.04 ± 0.01[b]
x_1	620 ± 5 nm	x_3	0.58 ± 0.01

[a] Parameters are defined in the caption to Figure 2. [b] This value is expressed as a multiple of the concentration of streptavidin required by assuming that all the gold particles are monodisperse with radius 7.6 nm and that each streptavidin occupies 20 nm^2 of the gold surface.

protein coated particles will move back into the particle-rich zone. Any other particles these protein-coated particles meet will stick to these protein coated particles, resulting in an aggregation. Our above assertion has been confirmed by the finding that at high streptavidin concentrations (above surface saturation) some initial aggregation is always observed (e.g. Figure 2 after 1.00 equiv). Further, such initial aggregation is more significant with poorer mixing techniques (e.g. injection and shaking at 2.00 equiv will yield aggregates between 100 and 200 nm−our observation of such lead us to develop the flow mixing method illustrated in Scheme 2).

From numerical integration, it is apparent that, with this system, the surface coverage of streptavidin exceeds 97% of its final value, while less than 3% of the biotin-modified gold nanocrystals have formed dimers. This permits a simplified analysis of the aggregation.

The rate of aggregation is dependent on the rate of dimer formation (the K_{11} term in eq 5); thus, any measure of a rate of aggregation should show a dependence on $P(\text{stick}|\text{collide})(\alpha)$. The size of aggregates at late times is a good measure, in this case, of the rate of aggregation, provided that the time is sufficiently early that precipitation is not significant. Our experiments show that in this system, after 1000 s, precipitation is not a factor. This was confirmed by the finding that no deviation is measured on remixing the samples. Figure 2 shows the average aggregate size after 1000 s and a fit to the $P(\text{stick}|\text{collide})(\alpha)$ function. The fit gives good agreement on the true surface coverage of streptavidin. The fit suggests that the amount of streptavidin which can bind to a gold particle is 1.04 times that which one would predict on the basis of the

size of streptavidin and the gold particles. The number of blocking points of contact, *n*, resulting from the fit falls within the geometrically predicted range of 0.5−1.2. Further, the baseline value from the fit corresponds, as expected, to the unaggregated particles coated with streptavidin.

Conclusions

These results highlight the extra parameters which must be considered when dealing with aggregation of incompressible particles with fixed binding sites. In comparison with the work of Kisak et al, we see diffuse aggregates and steric effects influencing the kinetics. It would be interesting to see what effects the particle−protein size ratio would reveal. Unfortunately, the colloidal gold system is not easily applicable to such studies as its strong optical absorbance prevents the use of the higher concentrations required for larger particles, while wall effects prescribe a lower limit.

Acknowledgment. The authors thank the reviewers for their invaluable help in improving the clarity of the manuscript.

References and Notes

(1) Mirkin, C. A.; Letsinger, R. L.; Mucic, R. C.; Storhoff, J. J. *Nature (London)* **1996**, *382*, 607−609.
(2) Shenton, W.; Mann, S. *Adv. Mater.* **1999**, *11*, 449.
(3) Storhoff, J. J.; Mirkin, C. A. *Chem. Rev.* **1998**, *99*, 1849−1862.
(4) Alivisatos, A. P.; Johnsson, K. P.; Peng, X.; Wilson, T. E.; Loweth, C. J.; Bruchez, M. P., Jr.; Schultz, P. G. *Nature (London)* **1996**, *382*, 609−611.
(5) Loweth, C. J.; Caldwell, W. B.; Peng, X.; Alivisatos, A. P.; Schultz, P. G. *Angew. Chem., Int. Ed. Engl.* **1999**, *38*, 1808−1812.
(6) Kisak, E. T.; Kennedy, M. T.; Trommeshauser, D.; Zasadzinski, J. A. *Langmuir* **2000**, *16*, 2825−2831.
(7) Mann, S.; Shenton, W.; Li, M.; Connolly, S.; Fitzmaurice, D. *Adv. Mater.* **2000**, *12*, 147.
(8) Connolly, S.; Fitzmaurice, D. *Adv. Mater.* **1999**, *11*, 1202.
(9) Connolly, S.; Rao, S. N.; Fitzmaurice, D. *J. Phys. Chem. B* **2000**, *104*, 4765−4776.
(10) Bayer, E.; Wilchek, M. *Methods Enzymol.* **1970**, *18A*.
(11) Tausig, F.; Wolf, F. J. *Biochem. Biophys. Res. Commun.* **1964,** *14***,** 205.
(12) Alonso, M. E.; Aragona, H. *Org. Synth.* **1972**, *58*, 147−152.
(13) Green, N. M. Spectrophotometric determination of avidin and biotin. In *Methods in Enzymology*; McCormick, D. B., Wright, L. D., Eds.; Academic Press. New York, 1974; Vol.18A, pp 418−424.
(14) Smoluchowski, M. v. *Z. Phys. Chem.* **1917**, *92*, 129−168.
(15) Press, W. H.; Flannery, B. P.; Tenkolsky, S. A.; Vetterling, W. T. *Numerical Recipes in Pascal-The Art of Scientific Computing*; Cambridge University Press: Cambridge, U.K., 1996.